Electronic Supplementary Information

1.Characterization and analytical methods

X-ray diffraction (XRD) measurements were obtained using a Lab X XRD- 6100 X-ray diffractometer. Scanning electron microscopy (SEM) and energy dispersive X-ray (EDX) elemental mapping images were obtained from a Gemini SEM 300 scanning electron microscope (ZEISS, Germany) at an accelerating voltage of 5 kV. Transmission electron microscopy (TEM) images were obtained from a Zeiss Libra 200FE transmission electron microscope operated at 200 kV. X-ray photoelectron spectroscopy (XPS) measurements were performed on an ESCALABMK II X-ray photoelectron spectrometer. N_2 adsorption/desorption tests were performed on a Micromeritics ASAP 2460. UV–Vis spectra were obtained using a highly sensitive spectrometer (Maya2000-Pro, Ocean Optics, UK). The peaks were obtained by deconvoluting the Raman spectra using a multi-peak Voigt fit. Electron paramagnetic resonance (EPR) measurements were performed on a Bruker A300 spectrometer. For liquid chromatography-mass spectrometry (LC-MS) analysis, the liquid chromatography unit was an Agilent 1290 UPLC system, and the mass spectrometry unit was an Agilent Q-TOF 6550 high-resolution mass spectrometer. The electrospinning system (model SS-X3, Beijing Yongkang Leye Technology Development Co.), muffle furnace for pre-oxidation (model KSL-1200X, Hefei Kejing Materials Technology Co.), and tube furnace for annealing (model OTF-1200X, Hefei Kejing Materials Technology Co.).

The experiments utilized aquaculture wastewater collected from a pig farm located in Jianyang, Chengdu, Sichuan Province, China. The wastewater underwent pretreatment using a sequential process of solid-liquid separation, thick-thin fractionation, anaerobic digestion, SBR, MBR, and reverse osmosis within the farm's

treatment system. Specifically, sampling was performed from the MBR effluent without further pretreatment in the laboratory.

2. Evaluation of Reactive Oxygen Species Contribution

The primary reactive oxygen species (ROS) in the system include sulfate radical ($SO_4^{\bullet-}$), hydroxyl radical (•OH), singlet oxygen ($^1O_2$), and superoxide radical ($O_2^{\bullet-}$). Therefore, the degradation process in the Fe-O-HCNF/PMS system can be described using a mass-balance model based on Equation (1). [1]

$$-ln\frac{[C_t]}{[C_0]} = k_{SO_4^{\cdot-}}\int\left[SO_4^{\cdot-}\right]dt + k_{OH}\cdot\int[OH\cdot]dt + k_{O_2^1}\int\left[O_2^1\right]dt + k_{O_2^{\cdot-}}$$

(1)

Due to the relatively low reactivity of superoxide radical ($O_2^{\bullet-}$), its contribution to pollutant degradation is generally minimal.[2] Therefore, this study focuses on estimating the roles of sulfate radical ($SO_4^{\bullet-}$), hydroxyl radical (•OH), and singlet oxygen ($^1O_2$). Leveraging established methodologies, we employed atrazine （ATZ， $k_{\bullet OH,ATZ}$=3.0×10^{9}M^{-1}s^{-1}， $k_{SO_4^{\bullet-},ATZ}$=2.6×10^{9}M^{-1}s^{-1}， $k_{O_2^1,ATZ}$=4.0×10^{4}M^{-1}s^{-1}）[3], nitrobenzene （NB， $k_{\bullet OH,NB}$=3.9×10^{9}M^{-1}s^{-1}， $k_{SO_4^{\bullet-},NB}$=1.0×10^{6}M^{-1}s^{-1}）[4], and sulfamethoxazole （SMX, $k_{\bullet OH,SMX}$=8.5×10^{9}M^{-1}s^{-1}， $k_{SO_4^{\bullet-},SMX}$=1.61×10^{10}M^{-1}s^{-1}， $k_{O_2^1,SMX}$=2.0×10^{4}M^{-1}s^{-1}）[5-7] as characteristic probes to quantify the exposure concentrations of $SO_4^{\bullet-}$, •OH, and $^1O_2$, respectively, with an initial probe concentration of 10 mg/L for each. To eliminate interference from direct adsorption, Fe-O-HCN-containing the probe solution were first agitated for 5 minutes without

PMS addition. The degradation data of the three probes (**Fig. S16**) were then substituted into Eqs. (2)–(4), [8,9] and the cumulative exposure levels of ROS over the reaction period were determined via simultaneous equation solving. Finally, the relative contributions of each ROS to TC degradation were calculated using Eq. (5).[10]

$$-ln\frac{[C_{t,\ ATZ}]}{[C_{0,ATZ}]} = k_{SO^{\cdot}_4^-,ATZ}\int [SO^{\cdot}_4^-]dt + k_{OH\cdot,ATZ}\int [OH\cdot]dt + k_{O_2^1,ATZ}\int [O_2^1]dt$$

(2)

$$-ln\frac{[C_{t,\ SMX}]}{[C_{0,SMX}]} = k_{SO^{\cdot}_4^-,SMX}\int [SO^{\cdot}_4^-]dt + k_{OH\cdot,SMX}\int [OH\cdot]dt + k_{O_2^1,SMX}\int [O_2^1]dt$$

(3)

$$-ln\frac{[C_{t,\ NB}]}{[C_{0,NB}]} = k_{SO^{\cdot}_4^-,NB}\int [SO^{\cdot}_4^-]dt + k_{OH\cdot,NB}\int [OH\cdot]dt$$

(4)

$$f_{ROS} = \frac{k_{ROS,TC}\int [ROS]dt}{k_{SO^{\cdot}_4^-,TC}\int [SO^{\cdot}_4^-]dt + k_{OH\cdot,TC}\int [OH\cdot]dt + k_{O_2^1,TC}\int [O_2^1]dt}$$

(5)

$k_{\bullet OH,TC}$ =1.40×10^{10}M^{-1}s^{-1};[11] $k_{SO_4^{\bullet-},TC}$ = 6.0×10^{9}M^{-1}s^{-1}.[12]

Current research reports lack quantitative reaction rate constants for singlet oxygen ($^1O_2$), but our analysis successfully estimated the relative contributions of sulfate radicals ($SO_4^{\bullet-}$) and hydroxyl radicals (•OH) to TC degradation at 89.5% and 10.5%, respectively. This significant disparity clearly demonstrates sulfate radicals' dominant role in the oxidative degradation system compared to their hydroxyl radical counterparts.

3. Second-Order Reaction Rate Constant (K_2)

The second-order kinetic rate constant (k_2) is calculated as:

$$k_2 = \frac{1}{C_t} - \frac{1}{C_0}$$

Where: C_t = Pollutant concentration at time **t, (mM);**

C_0 = Initial pollutant concentration **(mM).**

4. Evaluation of the potential risks of intermediate products to aquatic ecosystems

Software Tool (T.E.S.T) based on the Quantitative Structure-Activity Relationship (QSAR) model to assess the acute toxicity (LC50 and LD50), developmental toxicity, and mutagenicity of tetracycline (TC) and its degradation intermediates. The detailed evaluation results are presented in Table S4.

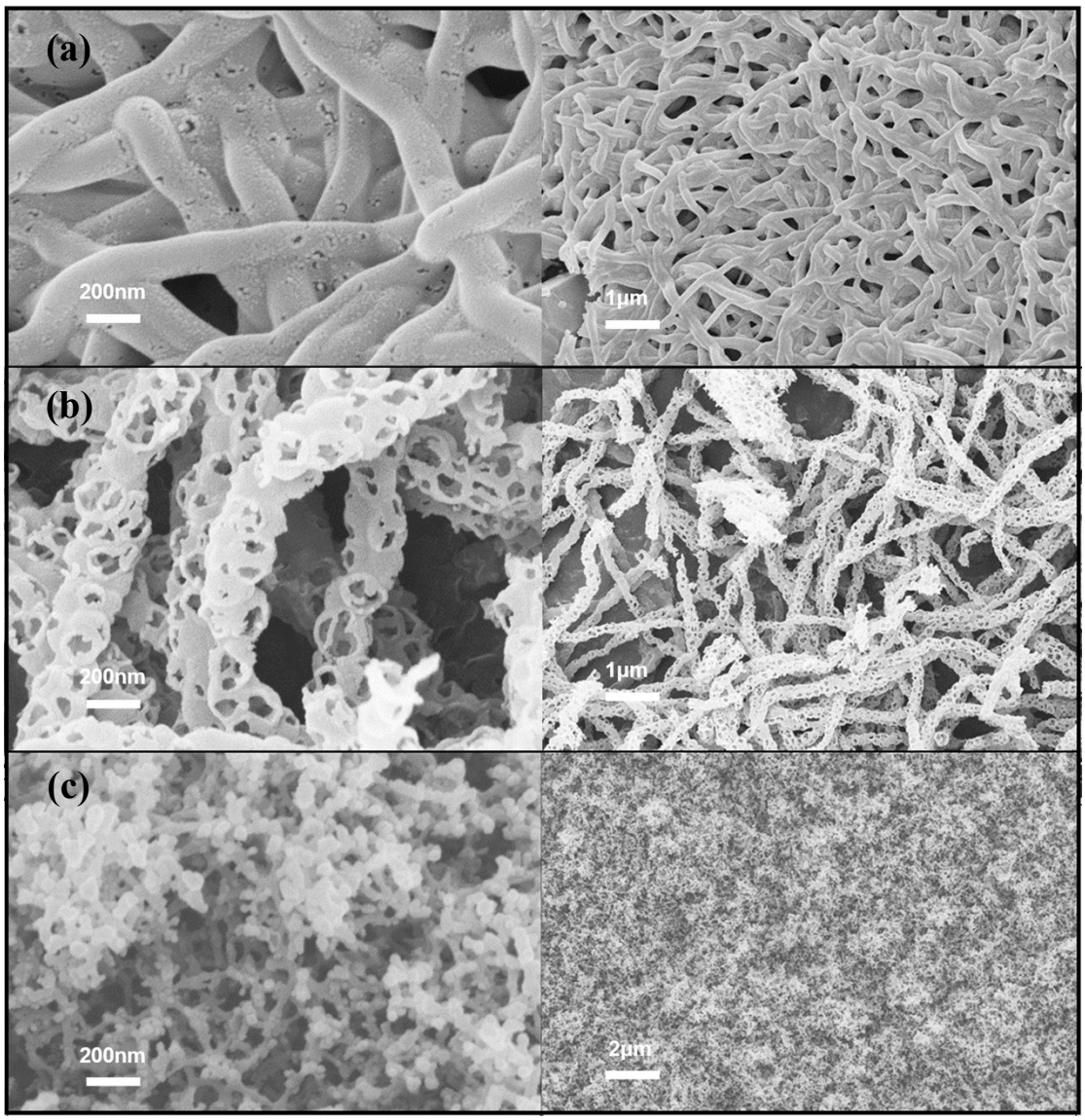

Fig. S1 SEM images of Fe-O-CNF (a), HCNF (b), and Fe-O-HC (c).

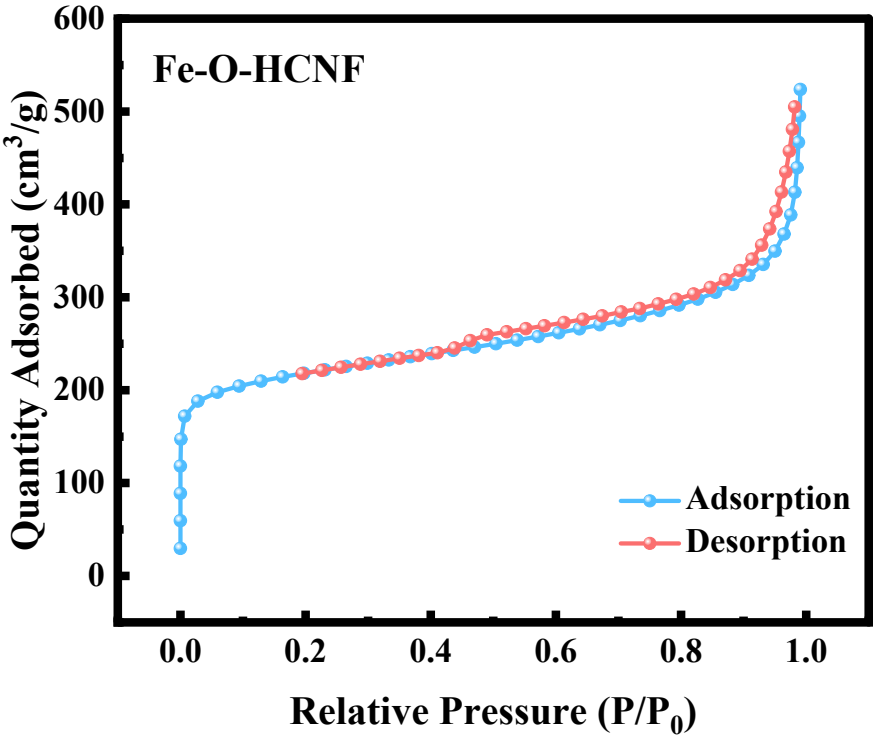

Fig. S2 N_2 adsorption-desorption isotherms of Fe-O-HCNF

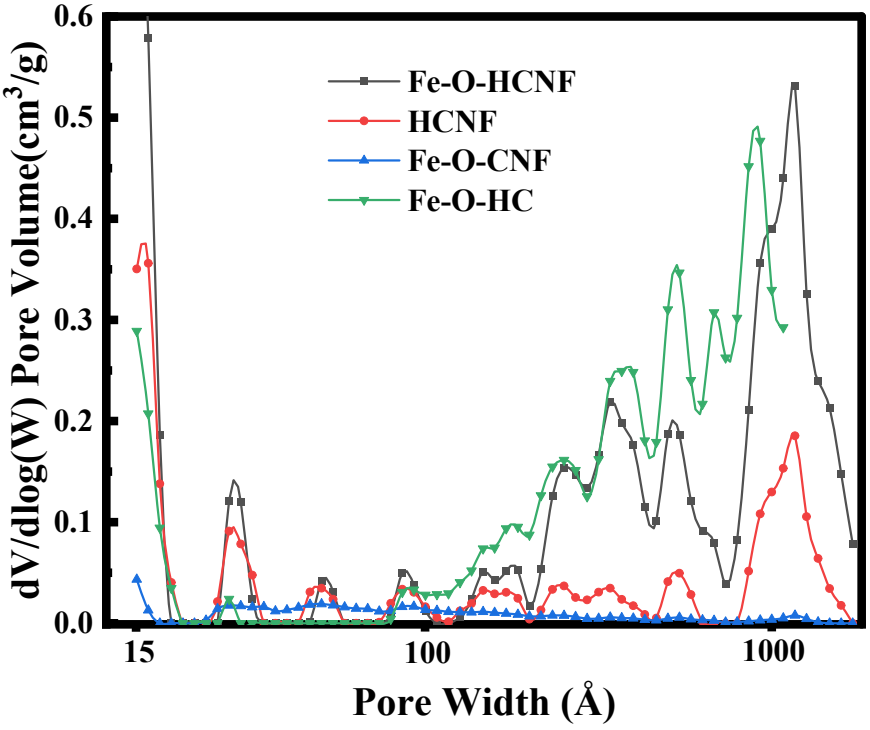

Fig. S3 pore size distribution of Fe-O-HCNF, HCNF, Fe-O-HC, Fe-O-CNF

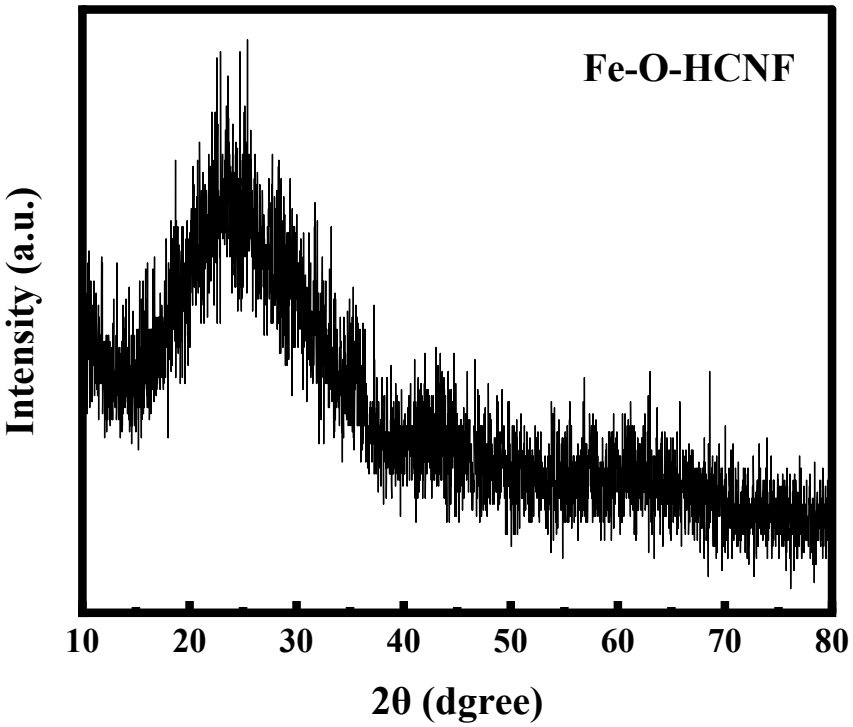

Fig. S4 XRD pattern of Fe-O-HCNF

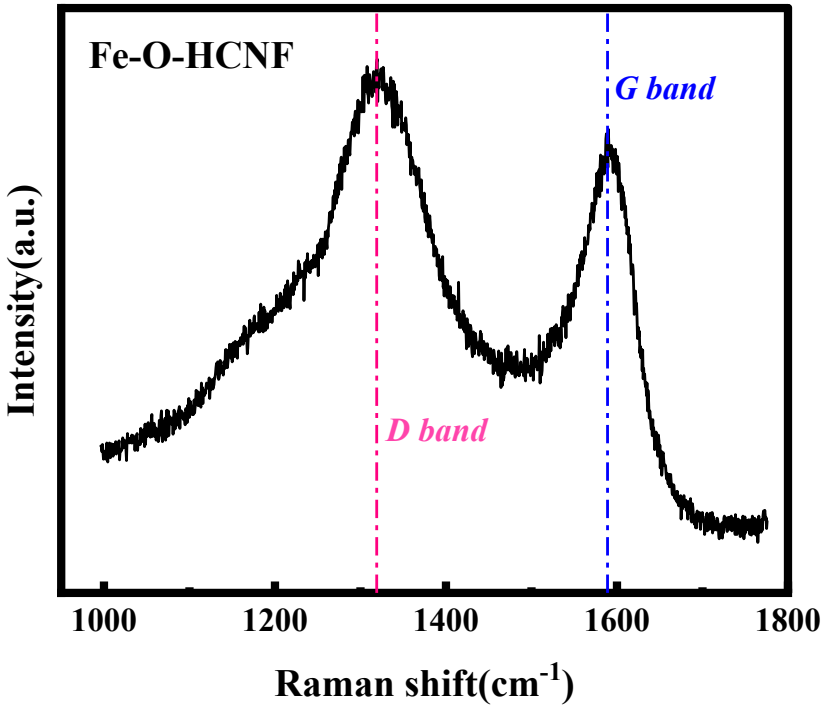

Fig. S5 Raman spectrum of Fe-O-HCNF

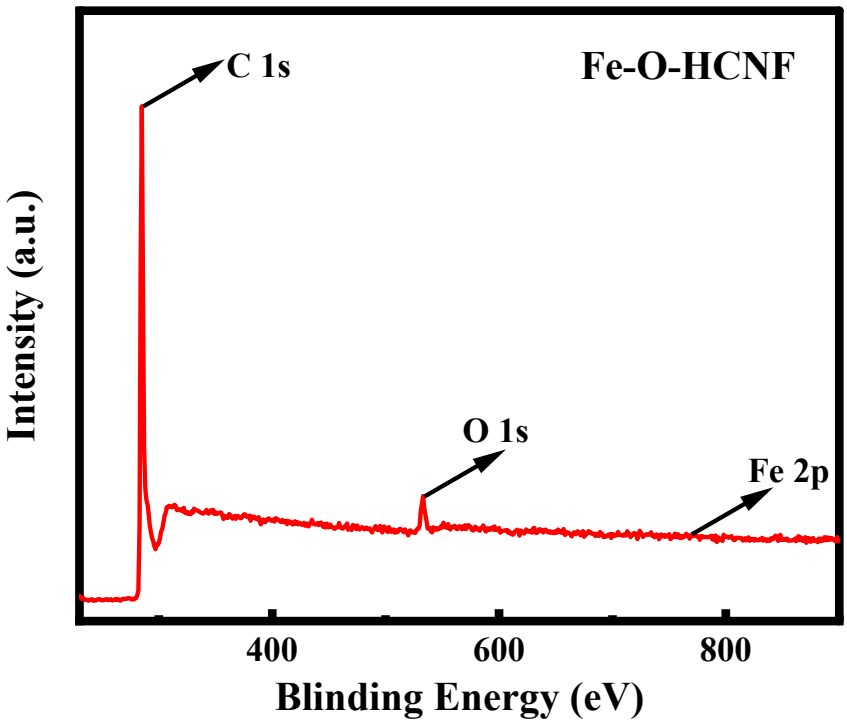

Fig. S6 XPS spectra survey scan of Fe-O-HCNF.

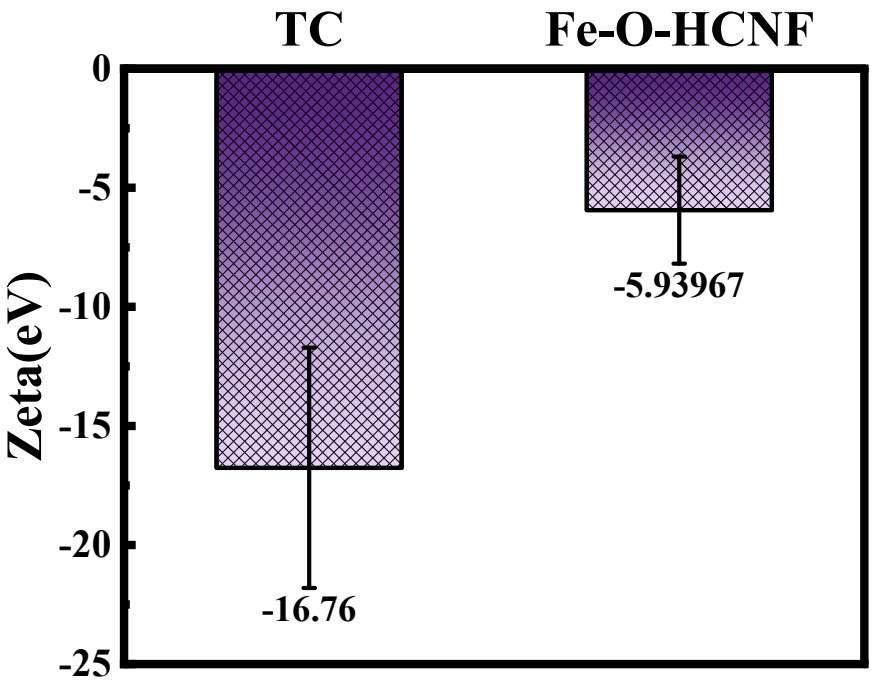

Fig. S7 Zeta potentials of Fe-O-HCNF and TC in UP water.

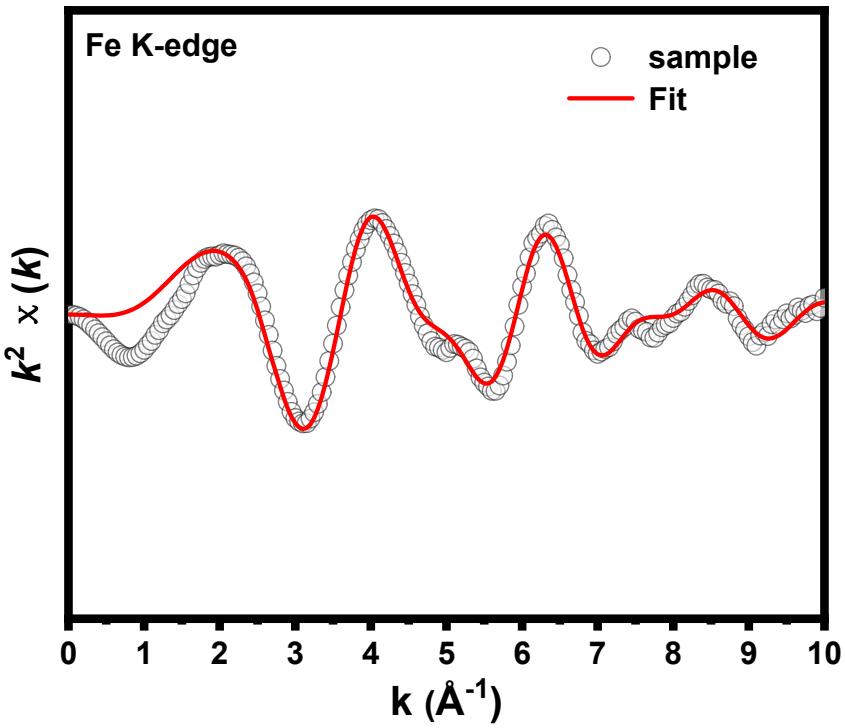

Fig. S8 K-edge EXAFS fit about k^2-weighted k-space for the Fe-O-HCNF

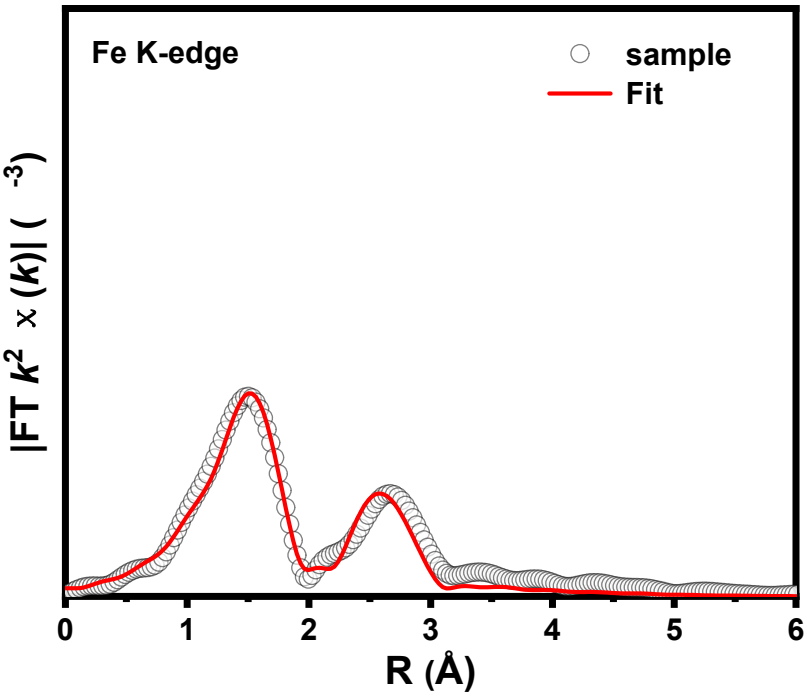

Fig. S9 Fourier transform EXAFS spectra and the corresponding curve-fitting result of the Fe-O-HCNF

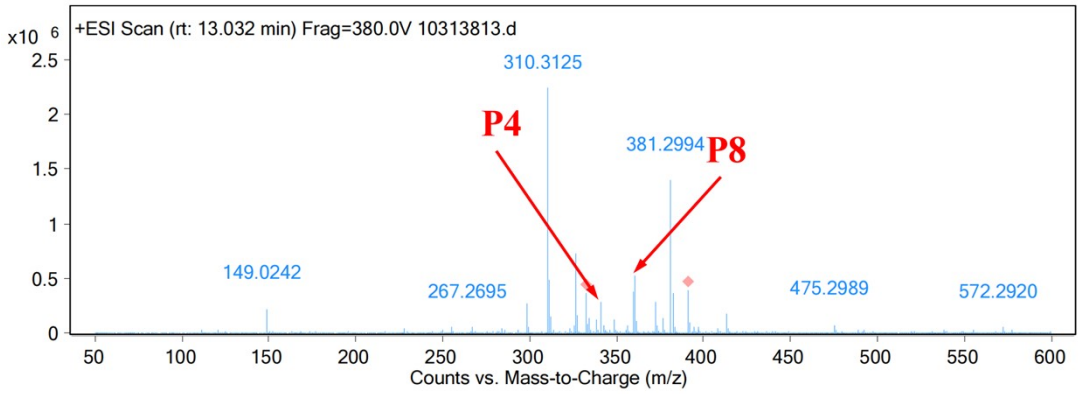

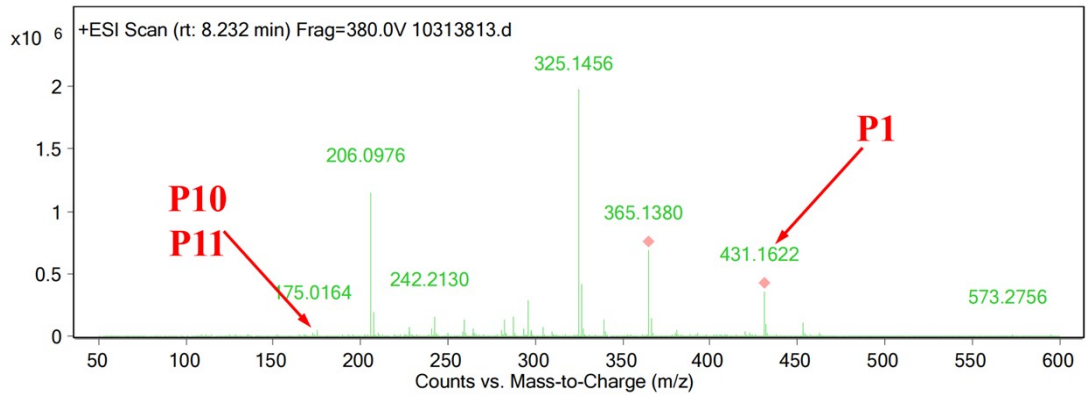

Qualitative Analysis Report

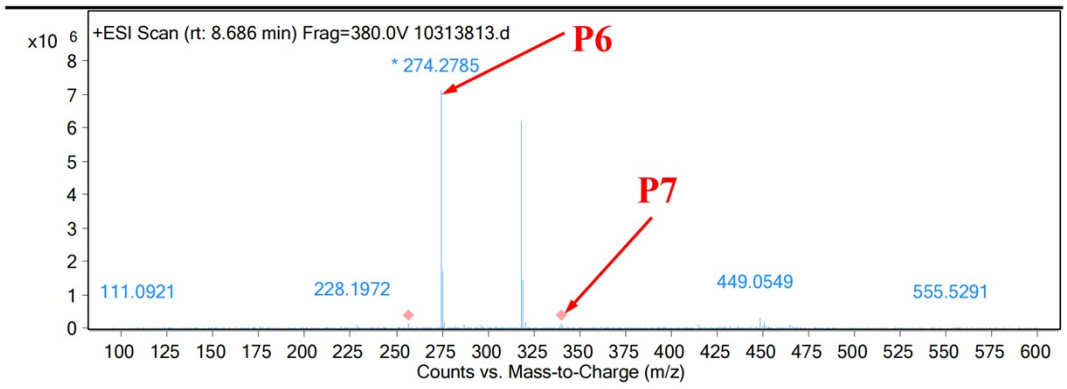

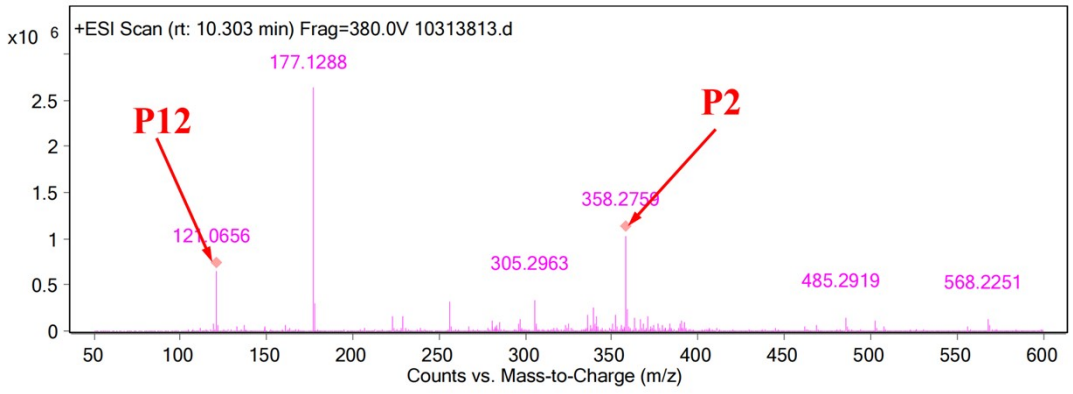

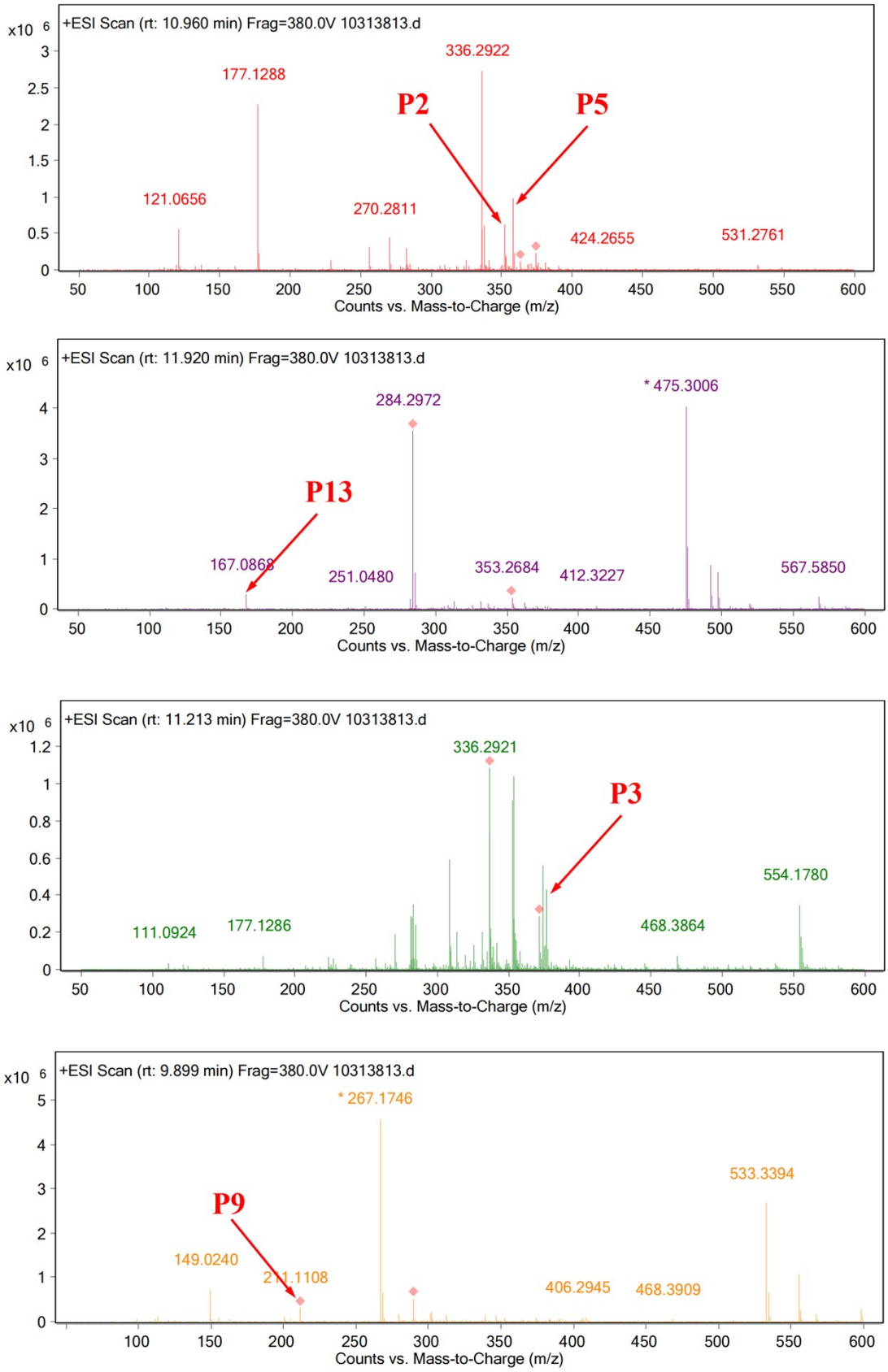

Fig.S10 TC degradation intermediates detected by HPLC-MS.

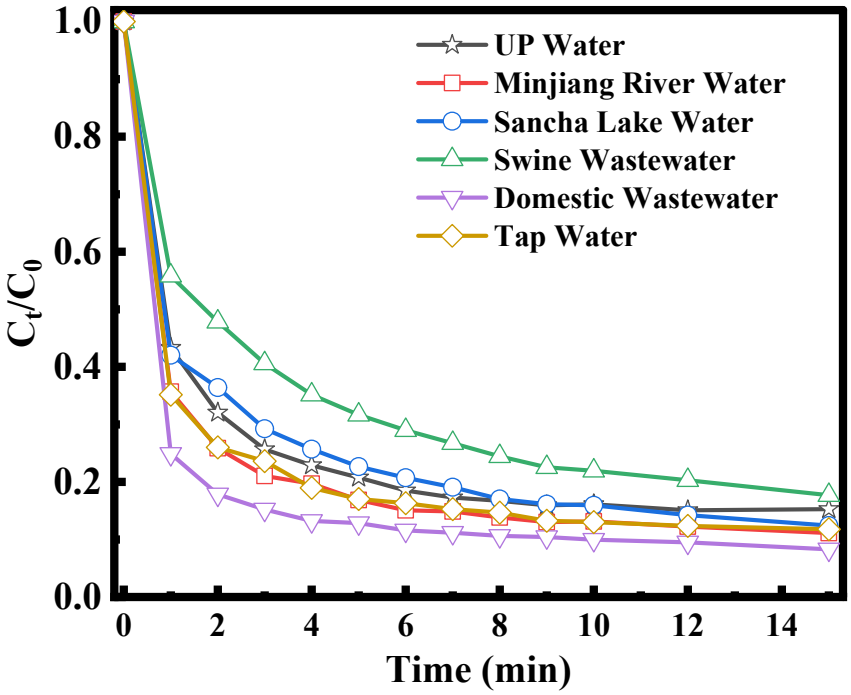

Fig. S11 Comparative TC degradation efficiencies by Fe-O-HCNF/PMS system in different real water matrices Experimental conditions: [TC] = 20 mg L^{-1}, [catalyst] = 0.02 g L^{-1}, [PMS] = 1.5 mM.

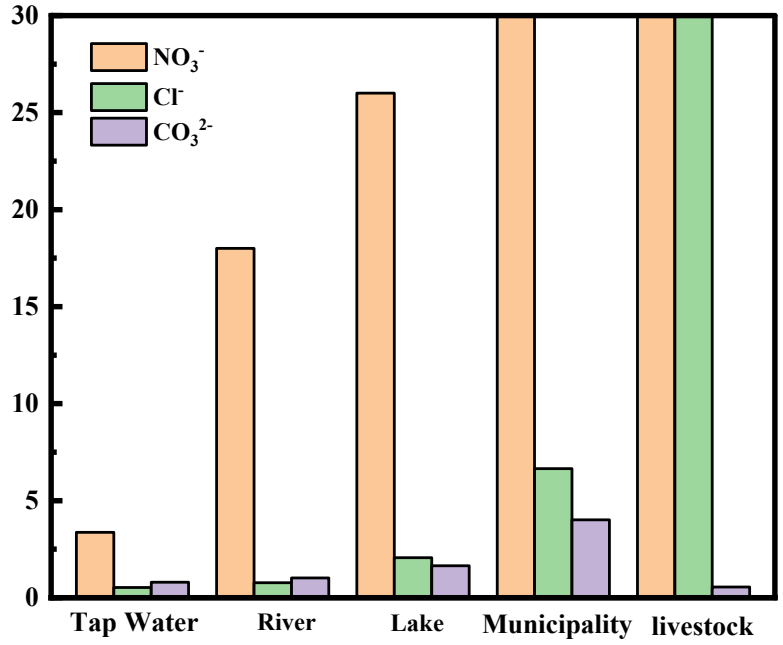

Fig. S12 Contents of common anions in various real wastewater matrices

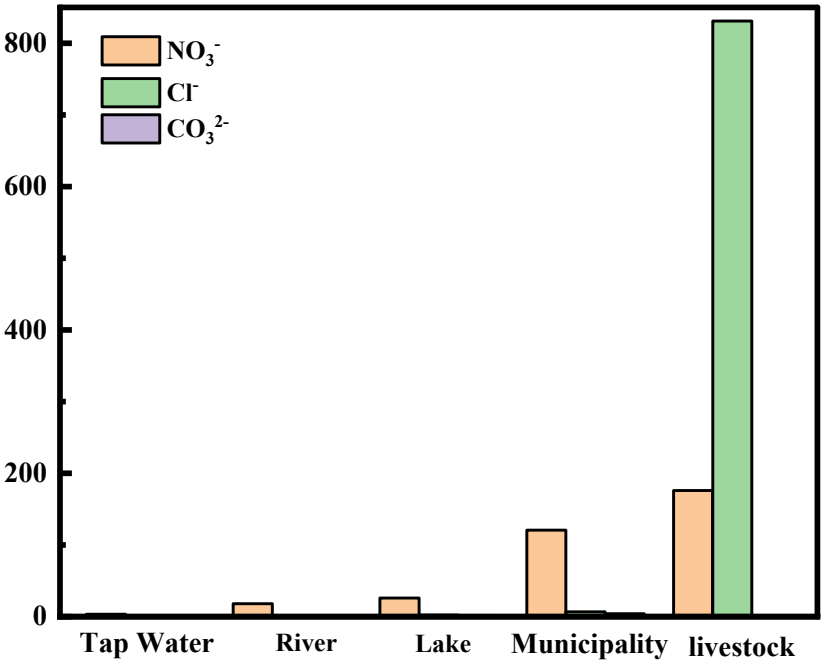

Fig. S13 Contents of common anions in various real wastewater matrices

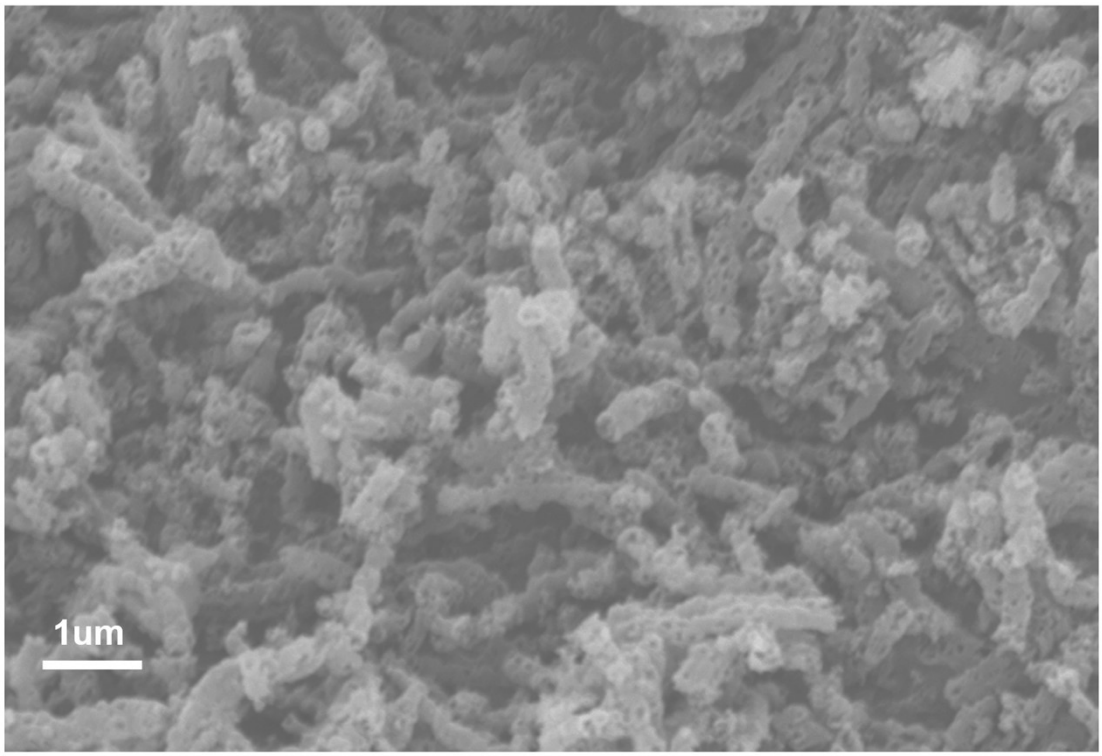

Fig. S14 SEM images of catalyst after 5 reuse cycles

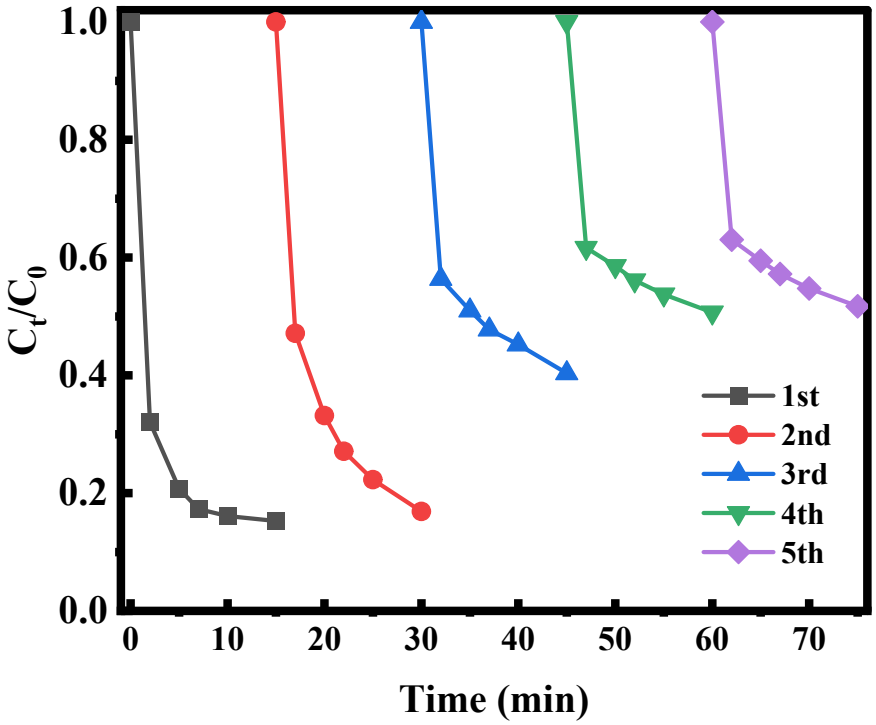

Fig. S15 Recyclability of Fe-O-HCNF catalyst for TC degradation. Experimental conditions: [TC] = 20 mg L^{-1}, [catalyst] = 0.02 g L^{-1}, [PMS] = 1.5 mM. unadjusted pH.

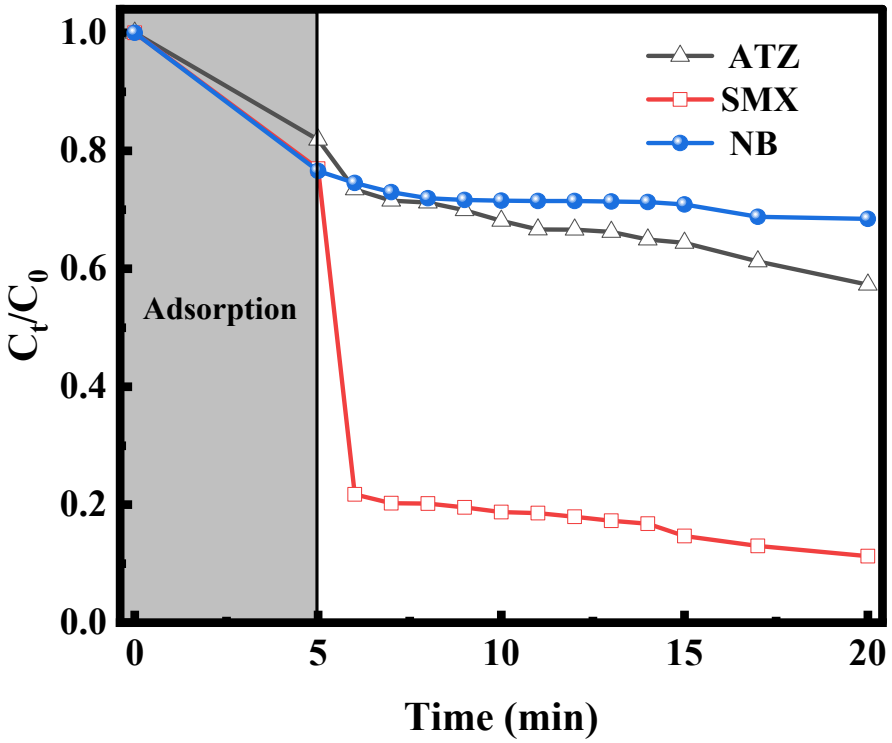

Fig. S16 Removal efficiency of various probes by the Fe-O-HCNF/PMS system. Experimental conditions: [probe] = 10 mg L^{-1}, [catalyst] = 0.02 g L^{-1}, [PMS] = 1.5 mM. unadjusted pH.

Table S1. The EXAFS data fitting results of Fe-O-HCNF.

Sample	Shell	Bond length (Å)	Coordination Number	σ2 (Å2)	E0 shift (eV)	R-factor
Fe-O-HCNF	Fe-O	1.99±0.01	4.1±0.6	0.008±0.002	-0.8±1.4	0.018
	Fe-Fe	3.02±0.02	3.7±0.7	0.017±0.006		

[a].The value of the amplitude reduction factor (S_0^2) was fixed to 0.70; [b]. Bond length is the interactomic distance; [c]. CN is the coordination number; [d]. σ2 is Debye-Waller factor (a measure of thermal and static disorder in absorber scatter distance); [e]. E_0 shift is edge-energy shift (the difference between the zero kinetic energy value of the sample and that of the theoretical model); [f]. R factor is used to value the goodness of the fitting.

Table S2. Kinetic fitting details of TC degradation under various PMS concentrations

NO	PMS concentration (mM)	R^2	Pearson's r	K_2	P(<F)
1	0	0.85461	0.92445	0.19665	1.70587×10^{-5}
2		0.836	0.91433	0.18916	3.1433×10^{-5}
3	0.1	0.94825	0.97378	0.84737	9.33441×10^{-8}
4		0.91203	0.955	0.80665	1.34659×10^{-6}
5	0.3	0.97332	0.98657	2.31645	3.3621×10^{-9}
6		0.94151	0.97031	2.350586	1.72732×10^{-7}
7	0.5	0.98377	0.99185	5.0251	2.78696×10^{-10}
8		0.96832	0.98403	4.84763	7.96348×10^{-9}
9	1	0.93948	0.96927	7.42226	2.04974×10^{-7}
10		0.95312	0.97628	7.31723	5.68694×10^{-8}
11	1.5	0.77795	0.88202	7.36514	1.4723×10^{-4}
12		0.85817	0.92638	7.46883	1.50425×10^{-5}
13	2	0.77359	0.87954	7.28982	1.62654×10^{-4}
14		0.76229	0.87309	6.7712	2.08712×10^{-4}

Table S3. Statistical table of recent reports on iron-based catalytic TC degradation

NO	Catalyst	Catalyst dosage	Oxidant	Degradation effect of TC	Ref.
1	Fe-O-HCNF	0.08g·L^{-1}	PMS	100% removed within 8 minutes★	This Work
2	FeS	0.2g·L^{-1}	PMS	100% removed within 10 minutes	13
3	$CoFe_2O_4$@BHC	0.1g·L^{-1}	PMS	100% removed within 10 minutes	14
4	Fe-N-modified porous carbon (Fe_5-NG)	0.1g·L^{-1}	PMS	100% removed within 12 minutes	15
5	Fe/N-CS900	0.2g·L^{-1}	PMS	100% removed within 15 minutes	16
6	Prc@Co-Mn_3O_4/Mil-53(Fe)	0.23g·L^{-1}	PMS	100% removed within 15 minutes	17
7	An expanded graphite-supported $CoFe_2O_4$ catalyst ($CoFe_2O_{4\text{-}EG}$)	0.06g·L^{-1}	PMS	100% removed within 30 minutes	18
8	The classical single-atom Fe-N_4 active neutral structure, Fe-MOFs	0.2g·L^{-1}	PMS	100% removed within 30 minutes	19
9	1Fe1N-C-800	0.6g·L^{-1}	PMS	100% removed within 30 minutes	20
10	xFe/BiOS	0.5g·L^{-1}	Light+PMS	90~100% removed within 30 minutes	21
11	ZIF-AB mixed matrix catalyst (MMC)	0.5g·L^{-1}	Light+PMS	99.9% removed within60minutes	22
12	Tri-metallic nitrogen-doped carbon nanoparticles (NCNPs)	0.6 g·L^{-1}	PMS	99.3% removed within15 minutes	23
13	CoFe alloy-decorated carbon nanofibers (CoFe/CF)	0.1g·L^{-1}	PMS	99% removed within 60 minutes	24
14	Fe -doped $CeNiO_3$	0.2 g·L^{-1}	PMS	98.5% removed within 60 minutes	25
15	FeNiP	0.1g·L^{-1}	PMS	98.36% removed within 60 minutes	26
16	α-Fe_2O_3/$BiVO_4$	/	Light+PMS	98% removed within90minutes	27
17	Magnetic $CuFe_2O_4$ nanoparticles immobilized on mesoporous alumina	0.5g·L^{-1}	PMS	97.9% removed within 10 minutes	28
18	A magnetic Fe tailings catalyst (MFT)	/	Light+PMS	97.88% removed within60minutes	29
19	Fe/Co loaded carbon ($Fe_{0.458}$/$Co_{0.124}$/PhBC)	0.2g·L^{-1}	PMS	97% removed within 7 minutes	30
20	$CuFeS_2$@FeS_2	0.4g·L^{-1}	PMS	96.70% removed within24 minutes	31
21	Fe-N-coordinated graphene-like honeycomb porous carbon	0.1g·L^{-1}	PMS	96.5% removed within 30 minutes	32
22	A sulfur-doped Fe/C catalyst (Fe@C–S)	0.2g·L^{-1}	PMS	96.4% removed within 40 minutes	33
23	A copper-iron-loaded layered porous catalyst (CFBC-0.5/1)	0.3 g·L^{-1}	PMS	96.2% removed within30 minutes	34

NO	Catalyst	Catalyst dosage	Oxidant	Degradation effect of TC	Ref.
24	$CuO/CuFe_2O_4/Fe_2O_3$（CCF）	$0.2g·L^{-1}$	PMS	95.5% removed within 60 minutes	35
25	Supramolecular organic frameworks (SOFs) CUGB-SOF-Fe	$0.067g·L^{-1}$	PMS	95.1% removed within 10 minutes	36
26	Fe, N co-doped graphene-like hierarchical porous carbon	$0.1g·L^{-1}$	PMS	94.4% removed within 60 minutes	37
27	Iron-doped biochar (Fe-BC)	$0.5g·L^{-1}$	PMS	94.3% removed within 60 minutes	38
28	Sulfur-decorated hematite nanoplates (SHNPs)	$0.2g·L^{-1}$	Light+PMS	93.89% removed within 30 minutes	39
29	MIL-88A(Fe)@CuS	$0.1g·L^{-1}$	PMS	93.1% removed within 40 minutes	40
30	$MnFe_2O_4/MoS_2$	$0.2g·L^{-1}$	PMS	92.9% removed within 30 minutes	41
31	Fe-N/C (active carbon)	$0.15g·L^{-1}$	PMS	90.23% removed within 20 minutes	42
32	Fe_7S_8 coupled tubular g-C_3N_4 (TCN)	$0.1g·L^{-1}$	PMS	90% removed within 15 minutes	43
33	Cu/MIL-101(Fe)	/	Light+PMS	89% removed within30minutes	44
34	Fe^0@NC	$0.05g·L^{-1}$	PMS	86% removed within 5 minutes	45
35	Fe-Co/NWCA	$0.16g·L^{-1}$	PMS	80% removed within 12 minutes	46

Table S4. TC and its degradation intermediates: acute toxicity and chronic toxicity.

Index	Fathead_minnow_LC50_(96_hr)_Consensus				Oral_rat_LD50_Consensus				Developmental_Toxicity_Consensus		Mutagenicity_Consensus	
	Exp_Value:-Log10 (mol/L)	Pred_Value:-Log10 (mol/L)	Exp_Value:mg/L	Pred_Value:mg/L	Exp_Value:-Log10 (mol/kg)	Pred_Value:-Log10 (mol/kg)	Exp_Value:mg/kg	Pred_Value:mg/kg	Exp_Value	Pred_Value	Exp_Value	Pred_Value
TC	N/A	5.69	N/A	0.9	2.74	2.46	806.96	1524.04	N/A	0.86	N/A	0.6
P1	N/A	4.82	N/A	6.31	N/A	2.35	N/A	1870.71	N/A	0.91	N/A	0.68
P2	N/A	5.19	N/A	2.31	N/A	2.63	N/A	834.98	N/A	0.76	N/A	0.93
P3	N/A	5.19	N/A	2.44	N/A	2.68	N/A	786.82	N/A	0.66	N/A	0.28
P4	N/A	5.65	N/A	0.77	N/A	2.36	N/A	1488.18	N/A	0.81	N/A	0.79
P5	N/A	4.88	N/A	4.75	N/A	2.46	N/A	1246.07	N/A	0.83	N/A	0.78
P6	N/A	4.91	N/A	3.38	N/A	2.74	N/A	500.14	N/A	0.78	N/A	0.5
P7	N/A	5.69	N/A	0.69	N/A	2.1	N/A	2692.59	N/A	0.86	N/A	0.69
P8	N/A	5.3	N/A	1.8	N/A	N/A	N/A	N/A	N/A	0.76	N/A	0.52
P9	N/A	3.4	N/A	90.24	N/A	1.78	N/A	3679.65	N/A	0.59	N/A	0.13
P10	N/A	4.84	N/A	2.52	N/A	N/A	N/A	N/A	N/A	0.62	N/A	0.4
P11	N/A	1.38	N/A	7305.92	N/A	N/A	N/A	N/A	N/A	0.53	N/A	0.31
P12	N/A	4.07	N/A	10.46	N/A	1.95	N/A	1359.86	N/A	0.62	N/A	0.21
P13	N/A	4.33	N/A	7.74	1.77	1.69	2823.16	3370	N/A	0.65	0	-0.05

References

1 L. W. Gao, Y. Guo, J. H. Zhan, G. Yu, Y. J. Wang, Assessment of the validity of the quenching method for evaluating the role of reactive species in pollutant abatement during the persulfate-based process. *Water Res.,* 2022, **221,** 118730.

2 Z. Luo, Y. Yan, R. Spinney, D. D. Dionysiou, F. A. Villamena, R. Xiao, D. Vione, Environmental implications of superoxide radicals: From natural processes to engineering applications, *Water Res.,* 2024, **261,** 122023.

3 L. Gao, Y. Guo, J. Zhan, G. Yu, Y. Wang, Assessment of the validity of the quenching method for evaluating the role of reactive species in pollutant abatement during the persulfate-based process, *Water Res.,* 2022, **221,** 118730.

4 Y. Lei, Y. Yu, X. Lei, X. Liang, S. S. Cheng, G. Ouyang, and X. Yang, Assessing the Use of Probes and Quenchers for Understanding the Reactive Species in Advanced Oxidation Processes, *Environ. Sci. Technol.*, 2023, **57,** 5433−5444.

5 R. Zhang, P. Sun, T. H. Boyer, L. Zhao, C. H. Huang, Degradation of pharmaceuticals and metabolite in synthetic human urine by UV, UV/H_2O_2 PDS, *Environ. Sci. Technol.*, 2015, **5**, 3056–3066.

6 S. P. Mezyk, T. J. Neubauer, W. J. Cooper, J. R. Peller, Free-radical-induced oxidative and reductive degradation of sulfa drugs in water: absolute kinetics and efficiencies of hydroxyl radical and hydrated electron reactions, *J. Phys. Chem. A.* 2007, **37**, 9019–9024.

7 A. L. Boreen, W. A. Arnold, K. Mcneill, Photochemical fate of sulfa drugs in the aquatic environment: Sulfa drugs containing five-membered heterocyclic groups, *Environ. Sci. Technol.*, 2004, **14**, 3933–3940.

8 Y. Guo, J. F. Long, J. Huang, G. Yu, Y. J. Wang, Can the commonly used quenching method really evaluate the role of reactive oxygen species in pollutant abatement during catalytic ozonation? *Water Res.,* 2022, **215,** 118275.

9 H. J. Wang, L. W. Gao, Y. X. Xie, G. Yu, Y. J. Wang, Clarification of the role of singlet oxygen for pollutant abatement during persulfate-based advanced oxidation processes: Co_3O_4@CNTs activated peroxymonosulfate as an example, *Water Res.,* 2023, **244,** 120480.

10 J. P. Liang, L. Fu, K. Gao, X. G. Duan, Accelerating radical generation from peroxymonosulfate by confined variable Co species toward ciprofloxacin mineralization: ROS quantification and mechanisms elucidation, *Appl. Catal. B*, 2022, **315,** 121542.

11 X. Ao, W. Sun, S. Li, C. Yang, C. Li, Z. Lu, Degradation of tetracycline by medium pressure UV-activated peroxymonosulfate process: Influencing factors, degradation pathways, and toxicity evaluation, *Chem. Eng. J.*, 2019, **361,** 1053-1062.

12 J. Jeong, W. Song, W. J. Cooper, J. Jung, J. Greaves, Degradation of tetracycline antibiotics: Mechanisms and kinetic studies for advanced oxidation/reduction processes, *Chemosphere,* 2010, **78,** 533-540.

13 Z. Zhao, L. Lin, S. Liu, Y. Chen, S. V. Daniels, Z. Xu, Z. Chen, H. Li, Y. Wu, L.

Guo, Q. Zheng, Z. Duan, W. Wang, B. Ni, Z. Xu and Y. Zhang, *Chem. Eng. J.*, 2024, **497**. 154682.
14 H. Chen, Z. Yu, W. Sun, T. Li, J. Zhang, Z. Qiu and M. Younas, *Sep. Sci. Technol.,* 2024, **351**, 128023.
15 S. Wang, Y. Song, Y. Wu, B. Wang, X. Gao, X. Zhu, J. Liu and P. K. Chu, *Adv. Sustainable Syst.,* 2025, **9**. 2500219.
16 Z. Yan, W. Gao, C. Zhong, Q. Jiao, X. Zhao and J. Liu, *Sep. Sci. Technol.,* 2024, **351**, 128075.
17 H. Zhu, J. Ma, P. Zhang, X. Hu, F. Xiao and Z. Ye, *Sep. Sci. Technol.,* 2025, **376**, 134187.
18 Q. Zhao, W. Li, L. Lv, S. Jiang, J. Zhang, C. Bai and X. Wang, *J. Mater. Chem. A,* 2025, **13**, 5919-5932.
19 S. H. Zhou, Y. Yang, R. D. Wang, Y. Cui, S. Ji, L. Du and F. Z. Jiang, *J. Colloid Interface Sci.,* 2025, **680**, 307-325.
20 B. Cai, S. Ouyang, J. Fan, C. Liu, Y. Zhang, Z. Wei, Z. Wang, X. Wang and H. Lei, *J. Environ. Manage.,* 2025, **388**, 126051.
21 L. Jiang, J. Song, Y. Hu, M. Yuan, X. Wang, K. Wang and W. Liu, *Sep. Sci. Technol.,* 2023, **323**, 124425.
22 D. Roy, P. Sarkar, A. Chowdhury, S. U. Zade and S. De, *J. Clean. Prod.,* 2024, **447**. 141548.
23 J. K. E. Erum, T. Zhao, Y. Yu and J. Gao, *SM&T.,* 2025, **45**. e01441.
24 M. Yang, X. Cheng, F. Geng, W. Han, P. Niu, L. Xie, Z. Li, Y.-Z. Zhang, D.-S. Zhang, J. Xu, X. Zhang and L. Geng, *J. Mater. Chem. A*, 2025, **13**, 4329-4342.
25 X. Tang, H. Ding, Q. Han, G. Zhou, R. Ma, Z. Xue, S. Yan, L. Zhang, J. Yin and E. H. Ang, *Mater. Horiz.,* 2025. DOI:10.1039/d5mh01099c
26 X. Pan, J. Pu, L. Zhang, X. Gong, X. Luo and L. Fan, *Environ. Res.,* 2024, **249**, 118362.
27 C. Hou, Q. Fan, M. Zhang, H. Wang, J. Li, Y. Liang, Y. Xuan, D. Wang and L. Wang, *J. Water Process. Eng.,* 2025, **70**. 107105.
28 Q. Li, J. Zhang, J. Xu, Y. Cheng, X. Yang, J. He, Y. Liu, J. Chen, B. Qiu, Y. Zhong and R. Sun, *Sep. Sci. Technol.,* 2024, **342**, 127076.
29 Y. Li, Y. Lu, X. Li, W. Zhong, B. Zhu, X. Tang and K. Liu, *Environ. Res.,* 2025, **276**, 121515.
30 B.-Y. Wang, H.-Y. Xu, J.-M. Lan, D.-Q. Liu, Y. Zhong and B. Li, *Sep. Sci. Technol.,* 2025, **361**. 131664.
31 Y. Li, Y. Lu, X. Li, W. Zhong, B. Zhu and K. Liu, *Chem. Eng. J.,* 2025, **509**. 161454.
32 M. Wu, Y. Tao, Y. Liu, S. Hou, T. Xiao, Q. Fu, G. Peng and L. Shi, *Sep. Sci. Technol.,* 2025, **354**, 129225.
33 J. Qian, Y. Zhang, Z. Chen, R. Yu, Y. Ye, R. Ma, K. Li, L. Wang, D. Wang and B. J. Ni, *J. Environ. Manage.,* 2023, **344**, 118440.
34 W. Shang, L. Wang, Z. Chen, D. Cheng, H. Liu, H. H. Ngo, J. Li, X. Cao, Y. Wang and J. Zhang, *J. Colloid Interface Sci.,* 2025, **689**, 137262.
35 J. He, L. Feng, T. Shi, F. Ni, L. Zhao, Y. Lei, Y. Liu, D. Fang, Z. Wei and F.

Shen, *Chem. Eng. J.,* 2024, **500**. 156759.
36 W. Li, Y. Hu, X. Liu, X. Cheng, Y. Dai, L. Yin and Q. Hua, *Sep. Sci. Technol.,* 2025, **359**, 130495.
37 S. Hou, H. Hu, Q. Fu, T. Xiao, J.-Q. Xie, S.-H. Chan, M. He, B. Miao and L. Zhang, *Sep. Sci. Technol.,* 2024, **333**, 125980.
38 W. Zuo, Y. Mao, W. Zhan, L. Li, Y. Tian, J. Zhang, W. Ma, C. Wu and L. Zhao, *J. Environ. Manage.,* 2024, **359**, 120979.
39 T. Guo, W. Yang, Z. Yang, Y. Li and G. Zhang, *Appl. Surf. Sci.,* 2025, **710**. 163870.
40 R. Ma, Z. Chen, W. Xu, R. Yu, Y. Zhang, F. Chen, X. Peng, B.-J. Ni and J. Qian, *J. Clean. Prod.,* 2024, **442**. 140885.
41 P. Xu, S. Xie, X. Liu, L. Wang, R. Wu and B. Hou, *Chem. Eng. J.,* 2024, **480**. 148233.
42 Z. Yan, X. Zhao, C. Zhong, W. Gao, Y. Feng and J. Liu, *Sep. Sci. Technol.,* 2025, **354**, 129489.
43 Z. Jiang, J. Wei, W. Yan, X. Niu, X. Cui, S. Li, J. Li and J. Wang, *Sep. Sci. Technol.,* 2025, **362**, 131862.
44 K. Zhang, S. Kang, R. Jia and C. Wang, *Environ. Res.,* 2025, **278**, 121664.
45 Y. Ji, F. Xu, K. Fang, H. Liu, X. Pan, Z. Jin, L. Zheng and L. Wang, *Environ. Technol. Inno.,* 2025, **38**. 104079.
46 S. Chen, J. Guo, P. Zhou, X. Xiao, K. Huo and J. Xu, *Sep. Sci. Technol.,* 2025, **355**, 129724.